Published in "EPL - Europhysics Letters 95(1): 12001, 2011"
which should be cited to refer to this work.

Production of ultracold neutrons from cryogenic $^2H_2$, O_2, and C^2H_4 converters

F. Atchison[1], B. Blau[1], K. Bodek[2], B. van den Brandt[1], T. Bryś[1], M. Daum[1], P. Fierlinger[1,3], P. Geltenbort[4], P. Hautle[1], R. Henneck[1], S. Heule[1,3], A. Holley[5], M. Kasprzak[1,6(a)], K. Kirch[1(b)], A. Knecht[1,3], J. A. Konter[1], M. Kuźniak[1,2], C.-Y. Liu[7], A. Pichlmaier[1], C. Plonka[4], Y. Pokotilovski[8], A. Saunders[9], D. Tortorella[10], M. Wohlmuther[1], A. R. Young[5], J. Zejma[2] and G. Zsigmond[1]

[1] *Paul Scherrer Institut (PSI) - CH-5232 Villigen PSI, Switzerland*
[2] *Institute of Physics, Jagiellonian University - Cracow, Poland, EU*
[3] *Institute of Physics, University of Zürich - Switzerland*
[4] *Institut Laue-Langevin (ILL) - Grenoble, France, EU*
[5] *North Carolina State University - Raleigh, NC, USA*
[6] *Stefan Meyer Institut for subatomic Physics, Austrian Academy of Sciences - Vienna, Austria, EU*
[7] *Indiana University - Bloomington, IN, USA*
[8] *Joint Institute for Nuclear Research - Dubna, Russia*
[9] *Los Alamos National Laboratory - Los Alamos, NM, USA*
[10] *Technical University München - München, Germany, EU*

Abstract – Ultracold neutrons (UCN) have been produced using the cold neutron (CN) beam FUNSPIN at SINQ on cryogenic oxygen (O_2), tetradeuteromethane (C^2H_4), and deuterium ($^2H_2$) targets. The target cell (40 mm long, fiducial volume about 45 cm^3) was operated between room temperature and 8 K and UCN were produced from gaseous, liquid and solid targets. UCN rates have been measured as a convolution of UCN production and transport out of the target and to the detector. At least within the accessible temperature range of this experiment, deuterium outperforms the other materials.

Introduction. – Efforts are underway worldwide to improve on the intensity and density of ultracold neutrons available to fundamental physics experiments[1]. The main two avenues use cold neutrons as an input onto a cryogenic converter, either superfluid helium [2] or solid ortho-deuterium [3]. Some ground-breaking work, demonstrating the potential of solid deuterium has been reported in [4–9]. In connection with the construction of a powerful deuterium-based UCN source at PSI, an extensive R&D program was pursued for the investigation of the relevant UCN source physics [10–16]. While different converter materials have been tested in the early days of UCN physics (see [17] for some history and references to the original work), the use of solid oxygen and solid tetradeuteromethane as potentially powerful UCN converters has been proposed only recently [18,19].

A UCN converter should provide a large cross-section for neutron "down-scattering" to lower energies, while at the same time "up-scattering" and absorption should be small or suppressed. While the down-scattering is governed by the available density of states, the up-scattering is affected by the actual population of excited states in a converter. This population at low temperatures is suppressed by the Boltzmann factor. It is usually helpful to characterize the properties of the converter by the UCN production rate R (dependent on the incoming

(a) Present address: University of Fribourg - Fribourg, Switzerland; E-mail: malgorzata.kasprzak@unifr.ch
(b) Also at ETH Zürich - Zürich, Switzerland; E-mail: klaus.kirch@psi.ch

[1] A solid $^2H_2$ UCN source is in the commissioning phase at PSI [1]. Other efforts are under way at Los Alamos National Lab, PNPI Gatchina, ILL Grenoble, RCNP Osaka, Mainz University, TU Munich, NC State University, TRIUMF and J-PARC.

neutron energy spectrum) and the UCN lifetime τ inside the converter material, such that the product with an incident cold neutron flux ϕ results in the equilibrium UCN density $\rho_{\rm UCN}$ inside the converter: $\rho_{\rm UCN} = R\phi\tau$. For deuterium $R \sim 10^{-8}\,{\rm cm}^{-1}$ has been calculated [3] and measured [11], while τ is limited to about 150 ms due to the unavoidable absorption of neutrons on deuterons. Practically, $\tau \sim 40$ ms [7] has been achieved experimentally so far, limited mostly by thermal and para up-scattering. For superfluid helium, the production rate has also been calculated [2] and measured [20] and, for a typical cold neutron beam spectrum, is about 1 order of magnitude lower than for deuterium, but $\tau \sim 900$ s (corresponding to the free neutron lifetime) can in principle be obtained in pure superfluid ^{4}He.

For good UCN production performance, low-loss materials (large τ) and systems with suitable down-scattering properties (large R) are required. The two novel cryogenic converter materials investigated in this work could fulfill these criteria. The absorption cross-sections of the constituent nuclei are relatively small ($\sigma^{\rm O}_{\rm abs} \sim 0.2$ mb and $\sigma^{\rm C}_{\rm abs} \sim 3.5$ mb leading to unavoidable loss rates due to absorption of about $1/400\,{\rm ms}^{-1}$ for O_2 and $1/40\,{\rm ms}^{-1}$ for C^2H_4) while the down-scattering could potentially make use of many more low-lying molecular states (for the case of C^2H_4) or the excitation of spin waves (for the case of O_2 in the antiferromagnetic α-phase). Contrary to the situation with superfluid helium and deuterium, where theoretical estimates were available at the time of the experiments, no conclusive predictions for the UCN production rates of O_2 and C^2H_4 exist to date.

Experiment. – The aim of this work was to test the UCN production performance of O_2 and C^2H_4 in comparison with $^2H_2$ (para-$^2H_2$ fraction 2%, compare [21]. A low para content is essential for the suppresion of UCN up-scattering, see [6,7,22]). The experiment was performed on the CN beam line for fundamental physics (FUNSPIN) [23] at the Swiss spallation neutron source SINQ. A schematic diagram of the experimental setup is displayed in fig. 1. The cryogenic and UCN parts were similar to the ones employed in [11], using the same gas system, cryogenic target (150 μm thin Al neutron beam windows, Ni coated on the inside of the CN entrance, see also [21]), UCN detector and UCN guide system with only minor modifications. The relevant changes in the setup as compared to [11] were the use of a different first UCN mirror (an Al foil coated with diamond-like carbon) and a time-of-flight (TOF) system for CN behind the first UCN mirror. Typical resolutions of the TOF system were 1–5%. After passing a 38 mm aperture and a 125 μm Zr vacuum window, CN from the FUNSPIN beam entered the 40 mm long target. Downstream of the target, a UCN guide system (Ni-coated stainless steel and Be-coated glass) was mounted in which after roughly 0.6 m a first mirror separated UCN (and some very cold neutrons, see [11]) from the CN beam by reflecting them

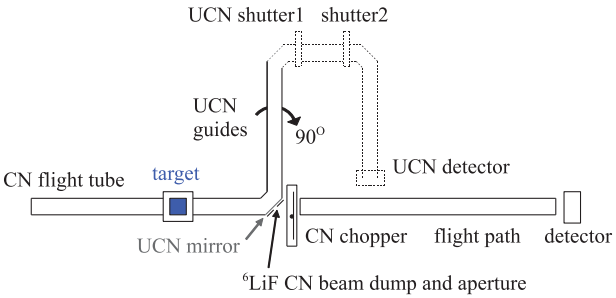

Fig. 1: (Colour on-line) The schematical setup (not to scale): the CN beam (for the incoming CN flux see fig. 2 in [13]) comes along a flight tube and hits the cryogenic target. Behind the target, UCN are reflected upwards by a mirror which is transparent for CN. The major part of the CN beam is dumped behind the mirror while the central fraction passes to the time-of-flight detection system. The UCN are simultaneously guided away from the CN beam axis to a well-shielded UCN detector (compare [11]).

upwards. The UCN were again reflected by 90◦ by a second mirror at about 1 m height into a horizontal guide section perpendicular to the axis of the incident beam; this helped to further filter the UCN spectrum and reduced beam-induced background in the detector system. UCN passed the 1.4 m long horizontal section and fell by about 1 m into a well-shielded ^{3}He gas detector. In order to reach the TOF system, CN passed through the UCN mirror (100 μm Al with diamond-like carbon coating), a 10 mm hole in the attached ^{6}LiF beam dump and a 100 μm Al vacuum exit window. The TOF system had a total flight path of 2830 mm and consisted of a one-disc-one-slit chopper (operated in air at 25 Hz and about 1/300 open to close ratio), a flight tube flushed with He to reduce neutron losses (2.5 m length, 16 μm Al entrance and exit windows), and a "thin" CN detector (the same as used in [23]). "Thin" refers to a small amount of ^{3}He in the counting gas which should result in a $1/v$ dependence of the detector efficiency on CN velocity v. The TOF system was used to monitor the CN beam intensity and spectrum. It also allowed measurement of the energy-dependent CN attenuation for various target conditions from which one can calculate total scattering cross-sections. These CN data have already been published in [16]. The produced UCN (in flow-through mode: both UCN shutters open) and transmitted CN have been detected for gaseous, liquid, and solid phases of $^2H_2$, O_2, and C^2H_4 at various temperatures. The information about temperatures of phase transitions have been collected in table 1.

Results and data analysis. – The data analysis follows the method used in [11] (for the measurements in the flow-through mode) with some modification due to, *e.g.*, a different normalization. Most notably, to determine the UCN production rates, I_m, in the sample, the number of detected UCN, N_{UCN}, is normalized to the transmitted

Table 1: Properties of $^2H_2$, O_2 and C^2H_4: temperatures (K) of phase transitions and neutron optical potentials V_F (Fermi potentials) of the solids.

	$^2H_2$	C^2H_4	O_2
Boiling point	23.5	112	90.2
Melting point	18.7	89.9	54.8
		$27.1 < I < 89.9$	$43.8 < \gamma < 54.4$
Solid Phases		$22.1 < II < 27.1$	$23.9 < \beta < 43.8$
		$III < 22.1$	$\alpha < 23.9$
V_F (neV)	~100	~177	~87

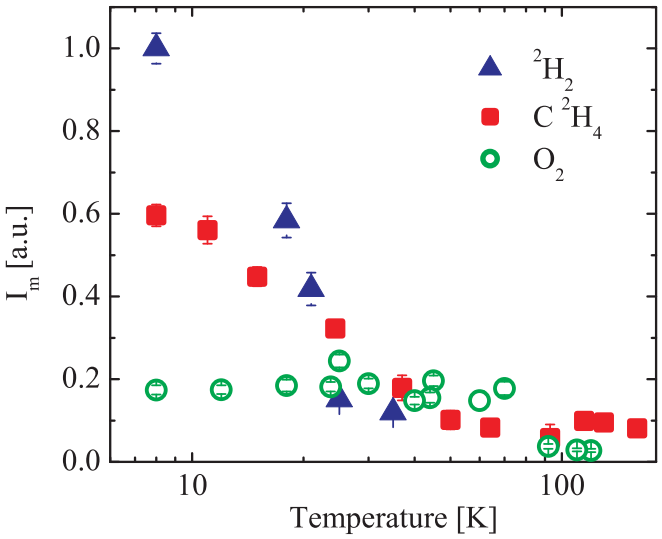

Fig. 2: (Colour on-line) The measured UCN production rates I_m for $^2H_2$, O_2 and C^2H_4 as a function of temperature of the cell. These rates are the detected UCN background corrected and normalized to the simultaneously detected, transmitted through the sample CN. The values shown in the figure are normalised to the measured UCN production rate for solid $^2H_2$ at 8 K which is (1.76 ± 0.08) $\times 10^{-4}$ detected UCN per detected CN. This corresponds to 350 ± 33 detected UCN per C^{-1}. The contribution of very cold neutrons (>250 neV) in the UCN spectrum, measured for the gaseous samples is $25 \pm 5\%$.

CN counts, N_{CN}, measured at the same time:

$$I_m = (N_{UCN} - N_b)/N_{CN}, \quad (1)$$

where N_b is the background UCN rate measured with empty target. The rates I_m are shown in fig. 2 for $^2H_2$, C^2H_4, and O_2 as a function of temperature. The rates I_m are the convolution of: i) the down-scattering cross-section in the material $\sigma^{CN \to UCN}$, ii) the extraction efficiency ε_e, iii) the transport efficiency ε_t which can be determined from the simulation. Since here the intention is to compare the UCN production in different materials, there is no need to determine the UCN production cross-sections as was done for $^2H_2$ in [11]. However, we have to take into account various transport efficiencies of the UCN spectrometer due to different optical potentials of the investigated materials. The efficiencies ε_t are obtained by simulations carried out using the GEANT4 UCN-Monte Carlo code [26], which tracks UCN through a detailed model of the UCN spectrometer system.

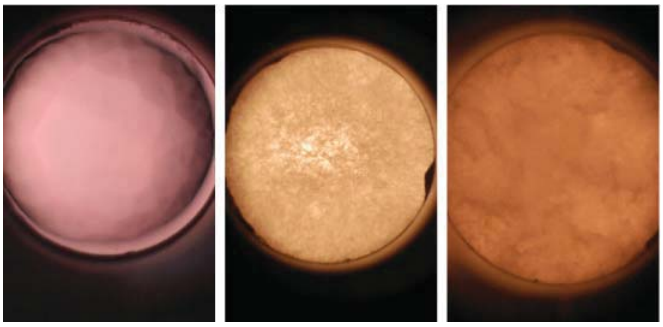

Fig. 3: (Colour on-line) The pictures of solid O_2 at different temperatures. From left: O_2 during solidification at 50 K, at 43 K, at 8 K illuminated with white light (the light is coming from a torch placed on the opposite side of the cell). The crystals are opaque and it is difficult to see what the structure is inside.

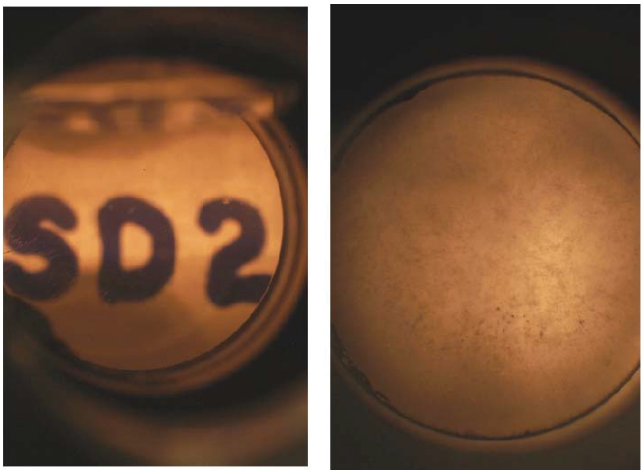

Fig. 4: (Colour on-line) The comparison of the transparencies of a $^2H_2$ crystal grown from the liquid (at 18 K, the picture on the left) and grown from the gas phase (at 12 K, the picture on the right). The detailed information about $^2H_2$ crystals growing can be found in [24,25].

The extraction efficiencies ε_e may in principle differ due to i) different elastic scattering and ii) different UCN lifetimes in the cryogenic solids. Ad-i): In a previous experiment we have shown that the scattering of UCN in $^2H_2$ can be severely influenced by the preparation and treatment of the crystal [12,24]. The information about the crystal quality is thus important and we have used optical inspection of the crystals to check the amount of the material in the target cell and to observe the quality of the crystals. Some example pictures of solid O_2, $^2H_2$, and C^2H_4 are shown in figs. 3, 4 and 5. Additionally we have measured the total scattering cross-section for cold neutrons (those

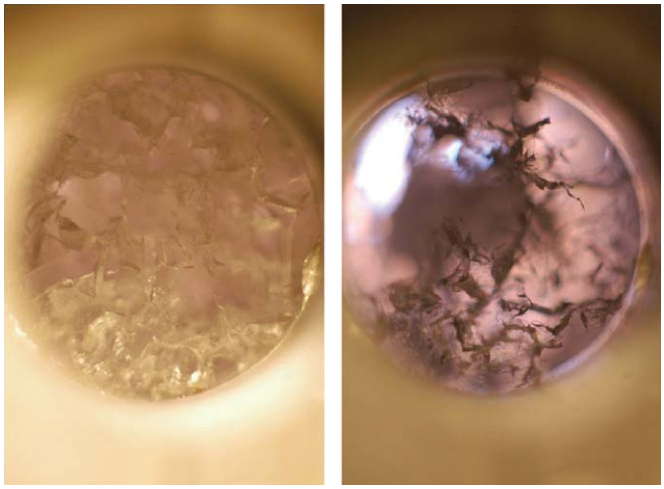

Fig. 5: (Colour on-line) The pictures of solid C^2H_4 at 22 K. The pictures have been taken with different focus, the picture on the right shows the structure on the surface and the one on the left inside the crystal.

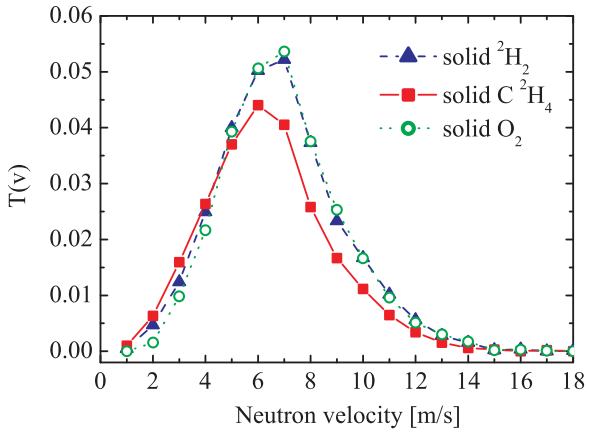

Fig. 6: (Colour on-line) The simulated transport efficiencies for solid $^2H_2$, O_2 and C^2H_4 inside the material. The simulation takes into account the Fermi potential of the materials.

data are used to normalize the UCN counts) which allows an estimation for the strength of elastic scattering in the CN energy region. Knowing the effect different UCN elastic scattering can have on the UCN yield measured in an experiment, we have set up our apparatus to be less sensitive to this scattering (see below). It was demonstrated experimentally that in the present setup the extraction of UCN from differently treated $^2H_2$ solids is the same within statistical error of ∼10% [11]. The UCN extraction from the target is strongly influenced by the solid angle of the capturing UCN guide behind the target. Therefore, in one extreme case with no elastic scattering, the last downstream millimeters of the target contribute the most although the least CN interactions occur in this region. In the other extreme, with strong elastic scattering, the transparency of the crystal is reduced and less UCN are initially produced in the relevant downstream part of the target. However, UCN from the higher-CN-intensity entrance region of the target diffuse more effectively towards the end of the target. Simulations have shown that these effects effectively cancel. Ad-ii): For $^2H_2$ the UCN lifetime in the solid at 8 K is sufficiently long to not influence the extraction. For C^2H_4 and O_2 dedicated measurements should be performed. However, the temperature dependence of I_m (see fig. 2) is flat for O_2 and flattening at low temperature for C^2H_4 and confirms that the UCN lifetimes in the solid do not strongly influence ε_e. We thus conclude from i) and ii) that ε_e is essentially the same for the three materials at low temperature and can be neglected here. Therefore, we correct the measured UCN production rates I_m only for the transport efficiencies. We introduce the function $T(v)$ to include the dependence of the average UCN production cross-section $\bar{\sigma}(v_f)$ on the final neutron velocity v_f, $\bar{\sigma}(v_f) = \bar{\sigma}^{CN\to UCN} f(v_f)$ where, $f(v) \sim v^2$, so that

$$T(v) = f(v)\varepsilon_t(v) \tag{2}$$

with the normalization condition

$$\int_{v_1}^{v_2} f(v)\,\mathrm{d}v = 1, \tag{3}$$

where v_1 and v_2 are the velocities *in* the target material that lead to UCN storable in the bottle (<250 neV). The distributions $T(v)$ for solid $^2H_2$, C^2H_4 and O_2 are shown in fig. 6. To calculate the correction factors, functions $T(v)$ are integrated over the neutron velocity range that contributes to the UCN stored in the bottle. For solid $^2H_2$ ($V_F \sim 100$ neV [14]) the neutron velocity lies in the velocity range 0 to 6.8 m/s (corresponding to the energy range 0–250 neV) and

$$T_{^2H_2} = \int_0^{6.8\ \mathrm{m/s}} T(v)_{^2H_2}\,\mathrm{d}v = 0.039. \tag{4}$$

In case of solid C^2H_4 at 8 K with the optical potential V_F of 177 neV the corresponding neutron velocity range is 0 to 5.8 m/s (energy range 0–173 neV):

$$T_{C^2H_4} = \int_0^{5.8\ \mathrm{m/s}} T(v)_{C^2H_4}\,\mathrm{d}v = 0.031. \tag{5}$$

Solid O_2 at 8 K has $V_F = 87$ neV and thus the velocity range is 1.6 to 7.1 m/s (energy range 13–263 neV):

$$T_{O_2} = \int_{1.6\ \mathrm{m/s}}^{7.1\ \mathrm{m/s}} T(v)_{O_2}\,\mathrm{d}v = 0.041. \tag{6}$$

The corrected UCN rates I_c (corresponding to relative production cross-sections) are calculated using

$$I_c = I_m/T \tag{7}$$

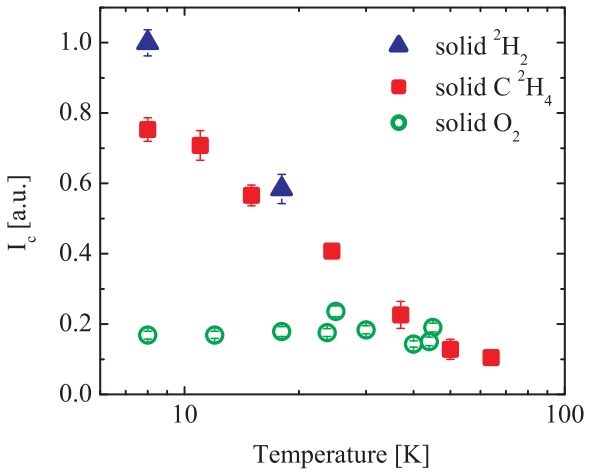

Fig. 7: (Colour on-line) The UCN production rates I_c for solid $^2H_2$, solid O_2 and solid C^2H_4. These rates are corrected for the transport efficiency (see fig. 6) measured UCN rates I_m. The assumption made here is that the UCN extraction efficiencies are the same for all three materials.

Table 2: UCN production rates I_c for solid $^2H_2$, O_2 and C^2H_4 at 8 K, corrected for the transport efficiency. The rates are assumed to be not affected by the UCN elastic scattering and up-scattering.

Material	I_c
$^2H_2$	1.0 ± 0.04
C^2H_4	0.75 ± 0.03
O_2	0.17 ± 0.01

and are shown in fig. 7 and for 8 K solids collected in table 2.

Conclusions. – The results obtained show that the UCN production rate at 8 K is the highest for solid $^2H_2$. The UCN production rate for solid C^2H_4 is 25% lower and for solid O_2 at 8.0 K the rate is six times smaller. The low UCN production rate for solid O_2 might be explained by the lack of magnetic structure (spin waves) in the crystals grown. In this case, the only possible channel for UCN production would be via phonon excitations. Comparing the calculated UCN densities produced in solid $^2H_2$ and O_2 (see fig. 7 in [18]), one can notice that the UCN density in solid O_2 without magnon excitations is about 6–7 times lower than for solid $^2H_2$. Important new insight from neutron scattering on solid O_2 [27] confirms that magnons do not contribute significantly under our conditions. It is possible that the CN scattering data do not compensate fully for the elastic scattering inside the crystal. The CN might not be sensitive to the damages of the crystal that are visible in the UCN energy region. The oxygen crystals grown in the experiment were opaque and the new research presented in [28] show that the optical transparency is minimizing the UCN loss. Other dedicated experiments (*e.g.*, investigating the transmission of UCN through the samples) are thus very important to understand the performance of oxygen as well as tetradeueromethane as UCN converters. In real UCN sources also other issues emerge due to high radiation, limited heat conductivity and thermal capacity of converters. Molecular carbon-containing moderators, for instance, encounter significant difficulties in use at high-power steady state or pulsed neutron sources by radiation damage leading to destruction and polymerization [29]. Solid $^2H_2$ is much less affected by radiation heating compared to the heavier elements and thus it is better suited for high power sources, such as at PSI, compare also [30].

* * *

The work was performed at the Swiss Spallation Neutron Source (SINQ), PSI, Switzerland. We acknowledge the outstanding technical support of W. Arrigoni, M. Meier and P. Schurter. We thank E. Widmann, A. Wokaun and J. Zmeskal for discussions. We acknowledge the support from Polish Ministry of Science and Higher Education, grant No. N N202 065436.

REFERENCES

[1] Anghel A. *et al.*, *Nucl. Instrum. Methods Phys. Res. A*, **611** (2009) 272.
[2] Golub R. and Pendlebury J. M., *Phys. Lett. A*, **62** (1977) 337.
[3] Golub R. and Böning K., *Z. Phys. B*, **51** (1983) 95.
[4] Altarev I. S. *et al.*, *Phys. Lett. A*, **80** (1980) 413.
[5] Serebrov A. *et al.*, *Nucl. Instrum. Methods Phys. Res. A*, **440** (2000) 658.
[6] Liu C.-Y., Young A. R. and Lamoreaux S. K., *Phys. Rev. B*, **62** (2000) R3581.
[7] Morris C. L. *et al.*, *Phys. Rev. Lett.*, **89** (2002) 272501.
[8] Saunders A. *et al.*, *Phys. Lett. B*, **593** (2004) 55.
[9] Serebrov A. *et al.*, *JETP Lett.*, **74** (2001) 302.
[10] Atchison F. *et al.*, *Phys. Rev. Lett.*, **94** (2005) 212502.
[11] Atchison F. *et al.*, *Phys. Rev. C*, **71** (2005) 054601.
[12] Atchison F. *et al.*, *Phys. Rev. Lett.*, **95** (2005) 182502.
[13] Atchison F. *et al.*, *Phys. Rev. Lett.*, **99** (2007) 262502.
[14] Altarev I. S. *et al.*, *Phys. Rev. Lett.*, **100** (2008) 014801.
[15] Altarev I. S. *et al.*, *Eur. Phys. J. A*, **37** (2008) 9.
[16] Atchison F. *et al.*, *Nucl. Instrum. Methods Phys. Res. A*, **611** (2009) 252.
[17] Ignatovich V. K., *The Physics of Ultracold Neutrons* (Clarendon Press, Oxford) 1990.
[18] Liu C.-Y. and Young A. R., arXiv:nucl-th/0406004v1.
[19] Pokotilovski Y., *ESS Special Expert Meeting, Wien, 2002.*
[20] Baker C. A. *et al.*, *Phys. Lett. A*, **308** (2003) 67.

[21] Bodek K. *et al.*, *Nucl. Instrum. Methods Phys. Res. A*, **533** (2004) 491.
[22] Serebrov A., *JEPT Lett.*, **59** (1995) 785.
[23] Zejma J. *et al.*, *Nucl. Instrum. Methods Phys. Res. A*, **539** (2005) 622.
[24] Kasprzak M., arXiv:nucl-ex/0407022v1.
[25] Kasprzak M., PhD thesis, Wien, 2008.
[26] Atchison F. *et al.*, *Nucl. Instrum. Methods Phys. Res. A*, **552** (2005) 513.
[27] Gutsmiedl E. *et al.*, arXiv:0911.4398v2 [nucl-ex].
[28] Frei A. *et al.*, arXiv:1006.2970v1 [nucl-ex].
[29] Shabalin E. P. *et al.*, *Part. Nuclei Lett.*, **5** (2002) 114.
[30] Bondoux D. *et al.*, *Nucl. Instrum. Methods Phys. Res. A*, **606** (2009) 637.